Properties of the gold oxides Au_2O_3 and Au_2O: First-principles investigation

Hongqing Shi,[1] Ryoji Asahi,[2] and Catherine Stampfl[1]
[1]*School of Physics, The University of Sydney, Sydney, New South Wales 2006, Australia*
[2]*Toyota Central R&D Laboratories, Inc., Nagauke, Aichi 480-1192, Japan*
(Received 1 September 2006; revised manuscript received 4 April 2007; published 25 May 2007)

Density-functional theory (DFT) calculations have been carried out using the generalized gradient approximation (GGA) to investigate the atomic and electronic structure and stability of the gold oxides Au_2O_3 and Au_2O. We find that Au_2O_3 is a semiconductor and is more stable than Au_2O, which is an endothermic system, and only metastable. The higher stability of Au_2O_3 is attributed to a greater hybridization of Au 5*d* and O 2*p* states throughout the valence-band region as compared to Au_2O. The highest energy, oxygen related normal vibrational mode is slightly higher in Au_2O_3 as compared to Au_2O. Au_2O is predicted by DFT-GGA to be metallic; calculations performed, however, using the screened-exchange local-density approximation find that it has a band gap of 0.83 eV; thus, it is a direct narrow-band-gap semiconductor.

DOI: 10.1103/PhysRevB.75.205125 PACS number(s): 71.15.Nc, 71.20.−b, 61.66.−f

I. INTRODUCTION

For many years, gold was considered inert as most gas molecules do not chemisorb, or readily dissociate, on the surface.[1,2] This view was changed by groundbreaking studies, which showed that nanosized Au particles supported on reducible metal oxides promote several catalytic reactions, e.g., the oxidation of carbon monoxide (e.g., Refs. 3 and 4 and references therein). Recently, the binary system, oxygen-gold, has attracted renewed interest because of the possible role it plays as intermediates in the preparation and operation of the supported gold nanoparticle catalysts for heterogeneous oxidation reactions (e.g., Refs. 1 and 5–10). Although gold is the most resistant noble metal to oxidation in air (or molecular oxygen), even at elevated temperatures, gold oxide (Au_2O_3) Refs. 11 and 12 can be synthesized under hydrothermal conditions with pressures of several 1000 atm (Ref. 13–15) such as those recently reported in the extended x-ray-absorption fine-structure study.[8] It can also be formed if highly reactive chemical environments are provided such as NO_2,[16] ozone,[16–19] or atomic oxygen (delivered, e.g., by molecular dissociation on a hot filament).[20] Gold oxide thin films have also been prepared by anodic oxidation within an electrochemical cell,[21–24] reactive sputtering from a gold target in an oxygen atmosphere,[25–27] treatment of a gold surface by exposure to an O_2 plasma,[5,28,29] oxygen-ion sputtering,[30] and pulsed laser deposition.[9] With thermal treatment, e.g., heating to around 450 K, Au_2O_3 decomposes, where Au_2O has been proposed as a possible intermediate.[28] Preparation of oxide films, AuO_x, with varying oxygen concentrations, $0.2<x<1.5$, have also been reported where the resistivity increases with oxygen content, reaching a maximum at $x=1.5$, corresponding to Au_2O_3.[6]

In order to better understand gold-based catalysts for heterogeneous oxidation reactions, a detailed understanding of the electronic properties of gold-oxygen compounds would be valuable. In the present paper, we investigate, through first-principles calculations, the atomic and electronic structure and the stability of Au_2O_3 and Au_2O, which to our knowledge has not been reported so far.

II. CALCULATION METHOD

The calculations are carried out using the *ab initio* density-functional theory (DFT) total-energy program VASP (Vienna *ab initio* simulation package),[31,32] where we use the projector augmented wave (PAW) method[33] and the generalized gradient approximation[34] (GGA) for the exchange-correlation functional. The wave functions are expanded in plane waves with an energy cutoff of 36.75 Ry (500 eV), and we use $3\times3\times9$ and $8\times8\times8$ **k**-point meshes for Au_2O_3 and Au_2O, respectively, for the Brillouin-Zone (BZ) integration, which yields 41 and 35 **k**-points in the irreducible part of the BZ. A Gaussian function is used with a temperature broadening parameter of $k_BT^{el}=0.2$ eV and the total energy is extrapolated to zero temperature. With these calculation parameters, our results are highly converged, as shown in the Appendix. The PAW potential is generated taking scalar relativistic corrections into account. Both spin-polarized and non-spin-polarized calculations yield identical results, confirming that these systems are not magnetic.

For Au_2O, which is predicted to be metallic using DFT-GGA and by the GGA+U approach (as mentioned below), we also calculate the electronic structure using a method that provides a more accurate description of the excited-state properties. In particular, we use the full-potential linearized augmented plane-wave method[35,36] with the screened-exchange local-density approximation (SX-LDA).[37,38] The SX-LDA approach, proposed by Bylander and Kleinman[39] and Seidl *et al.*[40] who showed that the method can be introduced as a particular case of the generalized Kohn-Sham framework, has been shown to yield good agreement of the calculated band gaps with experimental values.[37–40] It is less computationally demanding than the GW method[41] and also permits self-consistent determination of electronic structures as well as eigenfunctions.

To analyze the properties of the gold oxides, we calculate a number of quantities including the electronic band structure, partial density of states, and the difference electron density, which is defined as

$$n^{\Delta}(\mathbf{r}) = n(\mathbf{r}) - n^{Au}(\mathbf{r}) - n^{O}(\mathbf{r}). \quad (1)$$

Here, $n(\mathbf{r})$ is the total electron density of the optimized bulk gold oxide system, $n^{Au}(\mathbf{r})$ is the electron density of the gold

atoms only, which are held at the positions they have in the bulk oxide, and $n^{O}(\mathbf{r})$ is that of the oxygen atoms only, held at the positions they have in the bulk oxide. This quantity, $n^{\Delta}(\mathbf{r})$, then shows the regions in the bulk oxide where the electron density is depleted and increased, compared to its constituents.

The heat of formation of Au_2O_3 is calculated as

$$H^f_{Au_2O_3\ \mathrm{bulk}} = E^{\mathrm{tot}}_{Au_2O_3\ \mathrm{bulk}} - 2E^{\mathrm{tot}}_{Au\ \mathrm{bulk}} - \frac{3}{2}E^{\mathrm{tot}}_{O_2}, \qquad (2)$$

where $E^{\mathrm{tot}}_{Au_2O_3\ \mathrm{bulk}}$ and $E^{\mathrm{tot}}_{Au\ \mathrm{bulk}}$ are the total energies of Au_2O_3 bulk (per Au_2O_3 unit) and a bulk gold atom, respectively. $E^{\mathrm{tot}}_{O_2}$ is the total energy of the oxygen molecule. For Au_2O, the heat of formation is

$$H^f_{Au_2O\ \mathrm{bulk}} = E^{\mathrm{tot}}_{Au_2O\ \mathrm{bulk}} - 2E^{\mathrm{tot}}_{Au\ \mathrm{bulk}} - \frac{1}{2}E^{\mathrm{tot}}_{O_2}, \qquad (3)$$

where $E^{\mathrm{tot}}_{Au_2O\ \mathrm{bulk}}$ is the total energy of Au_2O bulk (per Au_2O unit). Here, a negative value of H^f corresponds to an exothermic system.

III. RESULTS

A. Bulk gold and the oxygen molecule

For bulk gold, which has the face-centered-cubic (fcc) structure, the calculated lattice constant is 4.175 Å and the bulk modulus is 132 GPa. The experimental values (at room temperature) are 4.08 Å and 170 GPa. Thus, the DFT-GGA result slightly overestimates the former (by 2.3%) and underestimates the latter (by 28.8%), similar to what has been reported for other metals (e.g., Refs. 42 and 43). These results agree very well with previous DFT-GGA calculations, where values of 4.19 Å and 132 GPa were reported.[44] The calculated cohesive energy of Au is 3.05 eV/atom, where we performed a spin-polarized calculation for the free atom, so that the spin-polarization energy (of 0.16 eV) is included. The value reported from VASP with a plane-wave basis set, using the local-density approximation (LDA), is 4.39 eV/atom (Ref. 45) and the experimental value is 3.81 eV/atom.[46] Thus, the DFT-GGA result underestimates the cohesive energy (by about 20%) and the LDA overestimates it (by about 15%).

For the oxygen molecule, we obtain an equilibrium bond length of 1.24 Å and a vibrational stretch frequency of 194 meV (1561 cm^{-1}). The binding energy is calculated (performing spin-polarized calculations) to be 3.14 eV per O atom. The corresponding experimental values are 1.21 Å, 196 meV (1580 cm^{-1}), and 2.56 eV, respectively.[47] The calculated bond length is slightly longer than the experimental value, and the vibrational frequency, slightly lower. The binding energy is overestimated (which is well known). These findings are typical for well-converged DFT-GGA calculations and similar values have been obtained in the literature, e.g., binding energies of 3.12 eV (Ref. 48) and 3.13 eV (Ref. 42) have been reported.

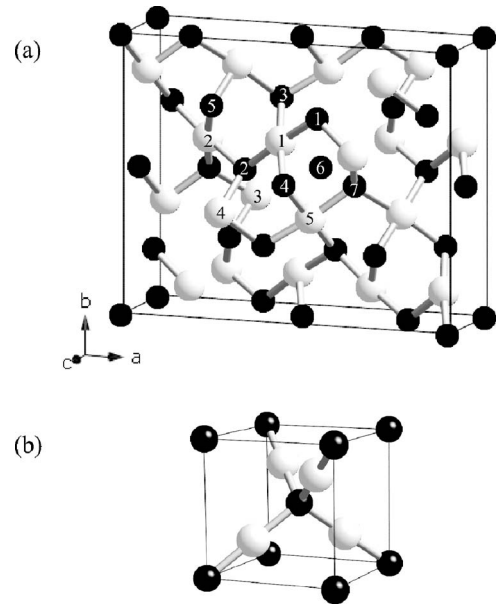

FIG. 1. Atomic structure of (a) the Au_2O_3 unit cell and (b) the cuprite bulk Au_2O unit cell. Oxygen and gold atoms are indicated by the small dark and larger gray circles, respectively. In (a), the atoms are labeled for discussion in the text. [The labels "1"–"7" on the O atoms correspond to labels O(1), O(1^a), O(1^b), O(2), O(2^a), O(2^g), and O(1^f) in Ref. 13.]

B. Bulk Au_2O_3 and Au_2O

1. Structural parameters

The atomic structure of bulk Au_2O_3 and Au_2O is shown in Figs. 1(a) and 1(b). We obtained the equilibrium geometry through minimization of the total energy, starting with the experimental structures. The (orthorhombic) unit cell of Au_2O_3 contains 40 atoms and is composed of a network of AuO_4 units that contain two types of oxygen atoms in crystallographically distinct sites: one type [the O atom labeled "4" in Fig. 1(a)], of which there are eight, is shared between two AuO_4 units (and is bonded to two Au atoms), and the other type [the O atoms labeled "1," "2," and "3" in Fig. 1(a)], of which there are 16, connect to three AuO_4 units (and are bonded to three Au atoms). The AuO_4 unit contains four Au–O bonds [see Au atom labeled 1 and O atoms labeled 1–4 in Fig. 1(a)]. The shortest (experimental) Au–O bond is 1.93 Å,[13,14] and the other three Au–O bonds are 2.01, 2.04, and 2.07 Å. There are also out-of-plane distortions (less than 8°) within the AuO_4 units, leading to additional deviations from an ideal square, planar symmetry.

Au_2O forms in the cuprite structure which has six atoms per cubic unit cell, where the oxygen atoms form a body-centered lattice, while the metal atoms are located on the vertices of a tetrahedron around each oxygen atom, forming a fcc lattice, as shown in Fig. 1(b).

For Au_2O_3, which has lattice constants a, b, and c, we carry out the structural optimization as follows: Starting with the experimental lattice constants and internal coordinates, we vary the lattice constant a to obtain the value that yields the lowest total energy, a_{opt}. During this procedure, at each step, the internal coordinates are scaled according to the

TABLE I. Lattice constants a, b, and c of Au_2O_3 obtained from the present study and experimental values (Ref. 13) (in Å). The deviations of the calculated values to experiment, in percent (Δ), are also given.

Lattice constant	This work	Expt.	Δ (%)
a	13.057	12.827	1.79
b	10.685	10.520	1.57
c	4.038	3.838	5.21

variation in a. At the determined a_{opt}, full atomic relaxation of the internal coordinates is performed. Next, we vary the lattice constant b with a fixed at the found a_{opt} (and internal positions) and c fixed at the experimental value to find the value of b which yields the lowest total energy, b_{opt}. During this procedure, at each step, the internal coordinates are scaled according to the variation in b. At the determined b_{opt}, full atomic relaxation of the internal coordinates is performed. The same procedure is followed in obtaining the corresponding value for c_{opt}. The whole process is repeated until the values of a_{opt}, b_{opt}, and c_{opt}, as well as the internal coordinates, remain unchanged. The forces on the atoms are relaxed to within less than 0.01 eV/Å. The calculated lattice constants for Au_2O_3, together with the experimental values, are listed in Table I.

The calculated values for a, b, and c are larger by 1.79%, 1.57%, and 5.21% with respect to the experiment, respectively. This trend of an overestimation is similar to that found above for bulk gold. A comparison of the calculated internal bond lengths and distances with experimental results is given in Table II, where overall, there is very good agreement with respect to the relative bond lengths.

The present calculated (and experimental[13]) angles of O1-Au1-O3, O3-Au1-O2, O2-Au1-O4, and O1-Au1-O4 (see Fig. 1) are 91.2° (89.6°), 94.4° (93.8°), 86.7° (86.9°), and 87.6° (89.2°), respectively, which also agree very well. The calculated structure of this open and complicated, low-symmetry system also exhibits good agreement with the results from extended x-ray-adsorption fine-structure (EXAFS) and multiple-scattering analysis,[8] as can be seen from Table II.

TABLE II. Calculated internal bond lengths and distances (see Fig. 1) and corresponding experimental values for bulk Au_2O_3 (in Å).

Bond/distance	This work	Expt.[a]	Expt.[b]
Au1-O1	2.05	2.01	
Au1-O2	2.07	2.04	
Au1-O3	2.11	2.07	
Au1-O4	1.99	1.93	2.00
Au1-O5	2.95	2.90	
Au1-O6	3.19	3.05	
Au1-O7	3.26	3.19	3.16
Au3-O2	2.97	2.81	2.91
Au1-Au2	3.42	3.35	
Au2-Au3	3.42	3.34	3.36
Au3-Au4	4.04	3.84	3.88
Au1-Au4	3.53	3.46	3.43
Au1-Au5	3.10	3.05	

[a]Reference 13.
[b]Reference 8, from an EXAFS and multiple-scattering analysis.

TABLE III. Calculated equilibrium lattice constant a_0 and internal distances for bulk Au_2O. $d_{Au\text{-}Au}$ and $d_{O\text{-}O}$ are the closest distances between two Au and two O atoms, respectively, and $b_{O\text{-}Au}$ is the bond length between oxygen and gold atoms (in Å).

	a_0	$d_{Au\text{-}Au}$	$d_{O\text{-}O}$	$b_{O\text{-}Au}$
This work	4.80	3.39	4.16	2.08
Theor.[a]	4.81	3.40		

[a]Reference 49.

The lattice constant for bulk Au_2O is 4.80 Å, which is in very good agreement with previous calculations (4.81 Å) reported using VASP and the GGA-PAW method, as also employed in the present work.[49] The Au-O nearest-neighbor distance is 2.08 Å. The nearest-neighbor distance between Au atoms in Au_2O is calculated to be 3.39 Å, which is larger than the (theoretical) value in bulk fcc gold which is 2.95 Å. These and other internal distances for bulk Au_2O are presented in Table III and lie between the range of values found in Au_2O_3.

2. Heat of formation and cohesive energy

The calculated heat of formation, per stoichiometric unit, for Au_2O_3 and Au_2O is −0.519 and 0.228 eV, respectively. The negative value for Au_2O_3 indicates an exothermic process, and the positive value for Au_2O, an endothermic process. Au_2O_3 is therefore more stable than Au_2O, which is only metastable with respect to the O_2 molecule and bulk Au. Reported experimental values of the heat of formation at the standard state (temperature of 273 K and 1 atm) per Au_2O_3 unit are −0.135 eV,[50] −0.0937 eV,[51] and −0.0353 eV.[52] Below, we consider the effect of temperature and O_2 pressure on the calculated (T=0 K) values, through the dependence of the oxygen molecule, and the vibrational contribution to the free energy of the oxides and bulk gold. For Au_2O, there are no experimental values with which to compare. The calculated cohesive energies for Au_2O and Au_2O_3 are 9.01 and 16.04 eV, respectively (corresponding to 3.00 and 3.21 eV/atom).

3. Normal vibrational frequencies

We calculated the zone-center (Γ-point) normal vibrational modes for Au_2O_3 and Au_2O by diagonalizing the dynamical matrix using an energy cutoff of 36.75 Ry (500 eV). The results for Au_2O are given in Table IV. Since Au_2O_3 has 40 atoms in the unit cell, this results in 120 modes which is too many to list. The highest-frequency mode is 581 cm^{-1} which is greater than that of Au_2O of 563 cm^{-1}. Using the calculated values of the vibrational frequencies of the oxides

TABLE IV. Normal (zone-center) vibrational modes for Au_2O, given in meV (and in cm^{-1} in parentheses). All frequencies are triply degenerate, except for the single 24.6 meV and doubly degenerate 9.5 meV modes.

Zone-center vibrational modes for Au_2O					
69.8 (563)	55.5 (447)	24.6 (198)	12.8 (103)	9.5 (77)	5.6 (45.1)

and bulk gold, together with the temperature and pressure dependence of the oxygen chemical potential, $\Delta\mu_O(T,p)$ [Eq. (4), below], we can estimate the contribution due to vibrational and entropic effects, at the standard state, to the calculated heat of formation (at $T=0$ K). The change due to pressure and temperature of the oxygen chemical potential is given by

$$\Delta\mu_O(T,p) = 1/2\left[\tilde{\mu}_{O_2}(T,p^0) + k_B T \ln\left(\frac{p_{O_2}}{p^0}\right)\right], \qquad (4)$$

where p^0 corresponds to atmospheric pressure and $\tilde{\mu}_{O_2}(T,p^0)$ includes the contribution from rotations and vibrations of the molecule, as well as the ideal-gas entropy at 1 atm. For $\tilde{\mu}_{O_2}(T,p^0)$, we use the experimental values from thermodynamic tables.[53] To estimate the contribution of the vibrational free energy (E^{vib}) and entropy (S^{vib}) for the oxides and bulk Au, $F^{vib}=E^{vib}-TS^{vib}$, we use the below expression involving a summation over the normal vibrational mode energies $\hbar\omega_i$,[54]

$$F^{vib}(T) = \sum_{i=1}^{3N}\left[\frac{\hbar\omega_i}{\exp(\hbar\omega_i/k_BT)-1} + \frac{1}{2}\hbar\omega_i\right] - Tk_B\sum_{i=1}^{3N}\left\{\frac{\hbar\omega_i}{k_BT}\left[\exp\left(\frac{\hbar\omega_i}{k_BT}\right)-1\right]^{-1} - \ln\left[1-\exp\left(\frac{-\hbar\omega_i}{k_BT}\right)\right]\right\}. \qquad (5)$$

Here, we calculate the normal vibrational frequencies for bulk Au using a 16-atom cell, and for Au_2O, we use a 24-atom cell (i.e., containing eight stoichiometric units). For Au_2O_3, we use the bulk unit cell (containing 40 atoms). The results are plotted in Fig. 2 for atmospheric pressure of oxygen. The dominant T and p dependence is given by $\Delta\mu_O$. At room temperature, the contribution due to vibrational free energy and entropy is 0.310 and 0.926 eV for Au_2O and Au_2O_3, respectively, resulting in calculated heats of formation of $0.228+0.310=0.538$ eV (0.179 eV/atom) and $-0.519+0.925=0.406$ eV (0.081 eV/atom), at the standard state. Thus, for Au_2O_3, compared to the experimental values which range from −0.135 eV,[50] −0.0937 eV,[51] and −0.0353 eV,[52] the theoretical value underestimates the heat of formation by around 0.44–0.55 eV per stoichiometric unit (or 0.09–0.11 eV/atom).

4. Electronic structure

We now investigate and compare the electronic structure of Au_2O_3 and Au_2O. In particular, we calculate the band structure, the density of states, and the difference electron-density distributions. The band structure is shown in the left panels of Figs. 3(a) and 3(b). The total density of states appears in the corresponding right-hand-side panels. It can be seen from the band structure of Au_2O_3 that it is predicted to be a semiconductor with a band gap of about 0.85 eV. Given that DFT-GGA (and LDA) typically underestimates the band gap,[55] the actual value can be expected to be notably larger.

The band structure of Au_2O is shown in Fig. 3(b) (left panel). It can be seen that at the Γ point, the valence and conduction bands overlap, making Au_2O metallic. This behavior, and character of the bands, is very similar to Ag_2O (Ref. 56) (which is isomorphic to Au_2O), in which DFT-GGA also yields no band gap, while experiments show that it is semiconducting with a band gap of about 1.3 eV.[57] We calculated the band structure of Au_2O using the GGA+U approach for a range of U values[58] and found no significant

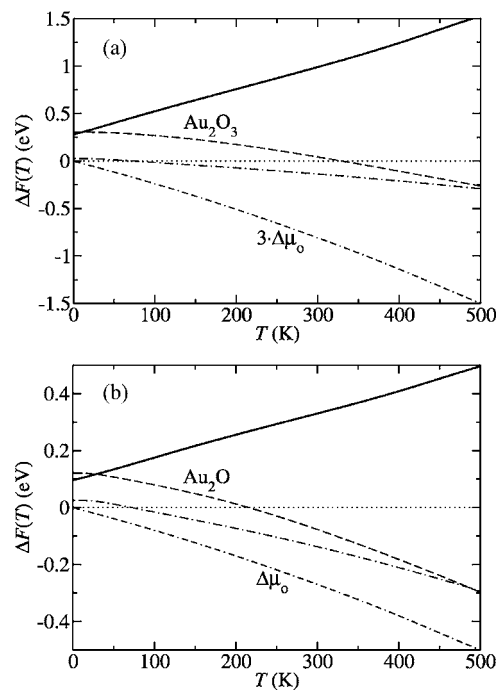

FIG. 2. The contributions at atmospheric pressure to the vibrational energy and entropy for bulk Au (per two atoms) and the gold oxides (per stoichiometric unit), as well as the pressure and temperature dependence of the oxygen chemical potential [per one O atom for Au_2O in (b) and per three O atoms for Au_2O_3 in (a)]. The dot-dashed line represents the contribution for bulk Au and those from the other systems are labeled. The full line represents the contribution of the Gibbs free energy due to pressure and temperature to the ($T=0$ K) heat of formation. Namely, it is the difference $\Delta F(T)=F^{vib}_{oxide}-F^{vib}_{2bulkAu}-n\Delta\mu_O$, where n is 1 or 3 for Au_2O and Au_2O_3, respectively.

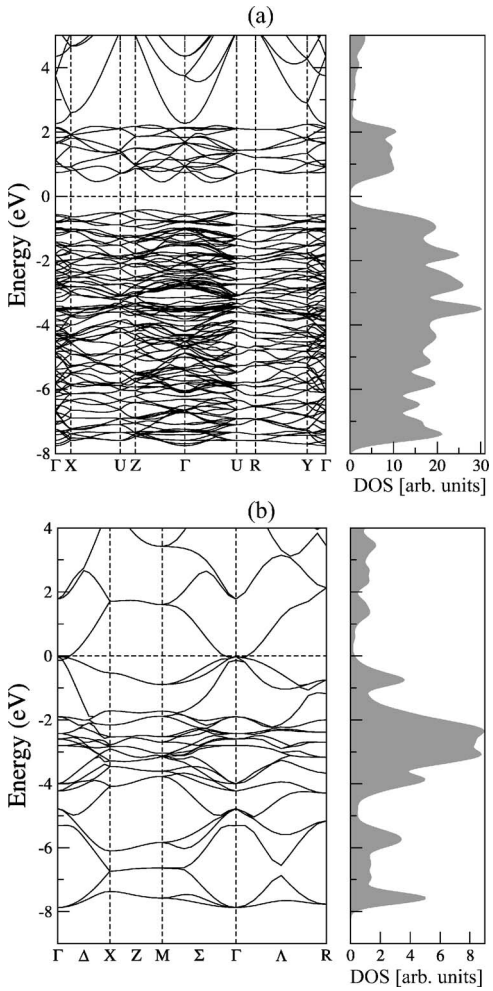

FIG. 3. The calculated band structure (left) and corresponding total density of states (DOS) (right) for (a) Au_2O_3 and (b) Au_2O. The energy zero corresponds to the Fermi level in (b) and is placed in the center of the band gap in (a).

change regarding the band gap. For Ag_2O, calculations employing the SX-LDA predict a direct band gap of 0.73 eV.[56] We also carried out calculations for the electronic band structure using the SX-LDA for Au_2O and similarly find it to be a semiconductor with a direct band gap of 0.83 eV, as can be seen from Fig. 4. Comparison of Figs. 3(b) and 4 shows that the main differences are that a notable band gap has opened up in the SX-LDA calculation and also that the valence band has become broadened; in particular, the four lowest-lying valeance bands (at the Γ point) in Fig. 3(b) are shifted down in energy so that they no longer appear in Fig. 4.

The projected densities of states (PDOSs) of the oxygen and gold atoms of Au_2O_3 and Au_2O are shown in Figs. 5(a) and 5(b), respectively, as calculated using DFT-GGA. For Au_2O, the PDOSs exhibit features in the energy range −8 to −5 eV, which involve a hybridization of Au 5*d* and O 2*p* states, and are largely of bonding character. In the region −2–0 eV, there are occupied antibonding states, also involving the Au 5*d* and O 2*p* orbitals. The Au 5*d* band is considerably narrower compared to bulk Au, which is due to the greater distance, and reduced overlap, between 5*d* states

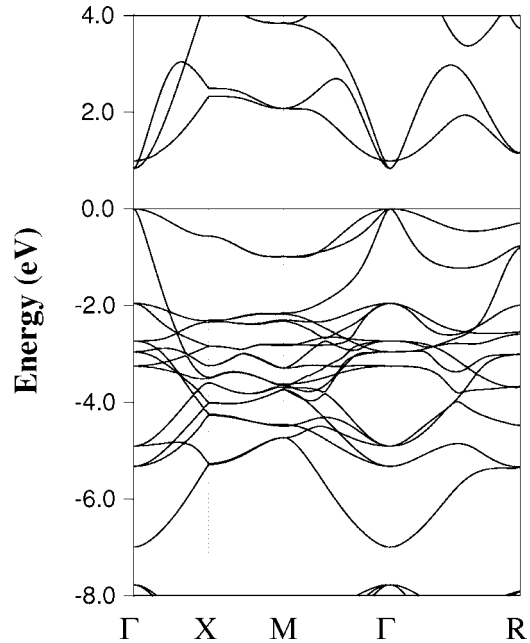

FIG. 4. The calculated band structure of Au_2O using the SX-LDA approach.

of nearest-neighbor Au atoms (the Au-Au distance in Au_2O is 3.39 Å versus 2.95 Å in bulk Au).

For Au_2O_3, the PDOSs for oxygen atoms O1, O2, and O3 [see Fig. 1(a)] are identical. These O atoms each bond to three Au atoms. Therefore, in the upper panel of Fig. 5(a), we only show the PDOS of O1 atoms. It can be seen that for the whole valence band, there is an overlap of Au 5*d* and O 2*p* states, with weight near the bottom (bonding) and top (antibonding) of the occupied bands. In the lower panel of Fig. 5(a), the PDOS of the O atom, O4, is shown. This O atom bonds with two Au atoms and has the shortest O-Au bond length. It can be noticed that here there is a stronger antibonding, and weaker bonding, feature compared to the oxygen atom O1 (and O2 and O3), indicating that the bond is weaker. The Au 5*d* band is notably broader for Au_2O_3 as compared to Au_2O, which may be attributed to the greater interaction with the oxygen atoms, which is also reflected in the greater stability of Au_2O_3.

To gain further insight into the nature of the bonding, we calculate the difference electron-density distributions for Au_2O_3 and Au_2O, as shown in Figs. 6(a) and 6(b), respectively. For Au_2O, there is a depletion of Au 5*d* states orientated along the O–Au–O bond axis, while there is an increase in electron density in the O 2*p* states. For Au_2O_3, there is also a clear depletion, but also a polarization, of the Au 4*d* states. There is an enhancement of electron density for the O 2*p* states, as well as polarization as reflected by the decrease in electron density in the *s*-like orbital "inside" the 2*p* states (closer to the atom center). Using the atom projected density of states, we find that the effective electron charge onthe O atoms of Au_2O is slightly greater than those of Au_2O_3, suggesting a more ionic bonding of the former.

IV. CONCLUSION

In the present paper, we have theoretically investigated the atomic and electronic structure and stability of Au_2O_3

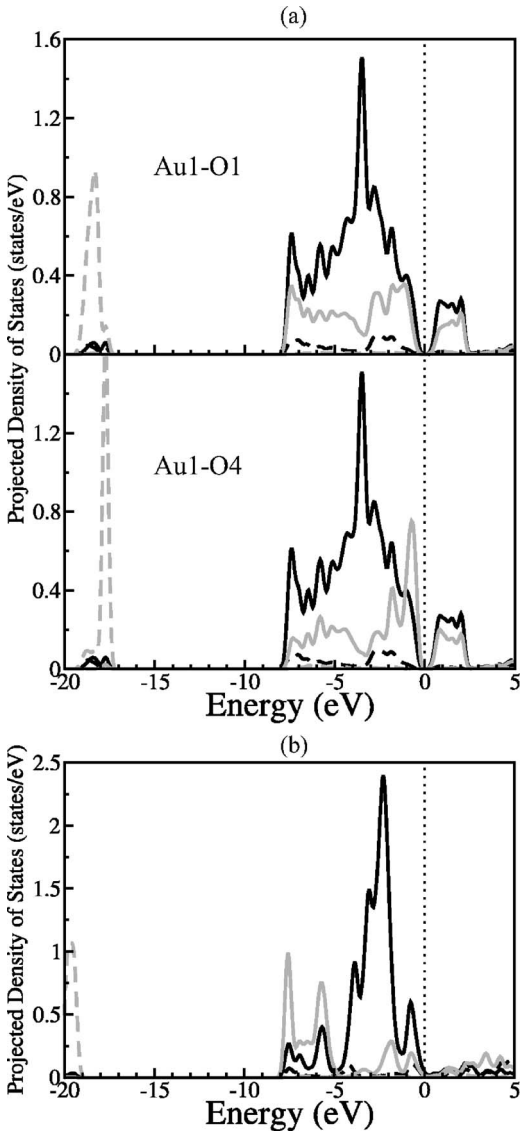

FIG. 5. Projected density of states for (a) Au_2O_3 and (b) Au_2O. The dark solid and dashed lines represent the Au 5*d* and 6*s* orbitals, respectively. The gray solid and dashed lines indicate the O 2*p* and 2*s* orbitals, respectively. The labels "Au1," "O1," and "O4" for Au_2O_3 correspond to the labels in Fig. 1(a). The Fermi energy is indicated by the vertical dotted line.

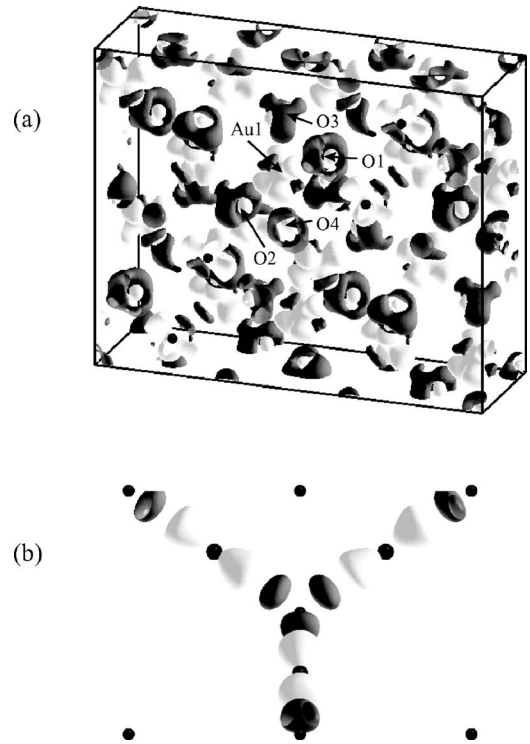

FIG. 6. The difference in electron density [see Eq. (1)] for (a) Au_2O_3 and (b) Au_2O. The dark isosurfaces represent an increase of electron density, and the light isosurfaces represent a depletion of electron density. The value of the electron density of the isosurfaces is $\pm 7.5\times 10^{-5} e/\text{Å}^3$. In (b), the black dots indicate the positions of Au and O atoms.

and Au_2O through first-principles DFT PAW-GGA calculations. We find that Au_2O_3 is more stable than Au_2O, which is consistent with experimental results. This is attributed to a greater hybridization of Au 5*d* and O 2*p* states over the valence-band region. We find that the effective electron charge on the O atoms of Au_2O is slightly greater than those of Au_2O_3, suggesting a more ionic bonding. Our results show that Au_2O_3 is a semiconductor, which is in line with experimental indications. Au_2O is predicted by DFT-GGA and the GGA+U approach to be metallic. Calculations performed, however, using the screened-exchange local-density approximation show that it is a semiconductor and yields a band gap of 0.83 eV. Au_2O therefore is a direct narrow-band-gap semiconductor.

ACKNOWLEDGMENTS

We gratefully acknowledge computing resources provided by the Australian Partnership for Advanced Computing (APAC) National Facility and the Australian Center for Advanced Computing and Communications (AC3). This work was supported by the Australian Research Council (ARC). We thank Klaus-Peter Bohnen for helpful discussions.

APPENDIX

For Au_2O_3, we tested **k**-point sets of $2\times 2\times 6$ and $3\times 3\times 9$ and found practically identical results, where the total energy differed by only 0.0018 eV per unit cell. We also tested two values of the temperature broadening parameter of $k_BT=0.2$ and 0.1 eV. The heat of formation changed by less than 0.001 eV and 0.003 eV for Au_2O_3 and Au_2O per stoichiometric unit, respectively.

We furthermore tested energy cutoffs of 400, 500, and 600 eV for the lattice constants and heat of formation (H^f) for Au_2O_3 and Au_2O. For Au_2O, we found that at 500 eV, H^f differed by only 0.0015 eV per stoichiometric unit compared to the value at 600 eV, while the value calculated at 400 eV differed by 0.019 eV compared to the value at 600 eV cutoff. For Au_2O_3, the deviations for 500 and 400 eV to that at

600 eV are 0.0044 and 0.0804 eV, respectively. With regard to the lattice constants, for both Au_2O_3 and Au_2O, the values are identical for cutoffs of 500 and 600 eV. For Au_2O, the lattice constant is 0.53% smaller at the 400 eV cutoff. For Au_2O_3, the *a*, *b*, and *c* lattice constants are 0.68%, 0.49%, and 2.55% smaller for the 400 eV cutoff. Thus, our results, as presented for the described calculation parameters in Sec. II are highly converged.

[1] R. Meyer, C. Lemire, Sh. K. Shaikhutdinov, and H.-J. Freund, Gold Bull. **37**, 72 (2004), and references therein.
[2] G. C. Bond and D. T. Thompson, Catal. Rev. - Sci. Eng. **41**, 319 (1999).
[3] M. Haruta, Gold Bull. **37**, 27 (2004), and references therein.
[4] M. S. Chen and D. W. Goodman, Science **306**, 252 (2004).
[5] B. Koslowski, H. G. Boyen, C. Wilderotter, G. Kastle, P. Ziemann, R. Wahrenberg, and P. Oelhafen, Surf. Sci. **475**, 1 (2001).
[6] F. Machalett, K. Edinger, J. Melngailis, M. Diegel, K. Steenbeck, and E. Steinbeiss, Appl. Phys. A: Mater. Sci. Process. **71**, 331 (2000).
[7] H. Tsai, E. Hu, K. Perng, M. Chen, J. C. Wu, and Y. S. Chang, Surf. Sci. Lett. **537**, L447 (2003).
[8] N. Weiher, E. A. Willneff, C. Figulla-Kroschel, M. Jansen, and S. L. M. Schroeder, Solid State Commun. **125**, 317 (2003).
[9] E. Irissou, M. C. Denis, M. Chaker, and D. Guay, Thin Solid Films **472**, 49 (2005).
[10] X. Y. Deng, B. K. Min, A. Guloy, and C. M. Friend, J. Am. Chem. Soc. **127**, 9267 (2005).
[11] M. Jansen and A. V. Mudring, in *Gold: Progress in Chemistry, BioChemistry and Technology*, edited by H. Schmidbaur (Wiley, Chichester, 1999).
[12] *Gmelin Handbook of Inorganic and Organometallic Chemistry*, Au-Gold Supplement Vol. B1 (Springer, Berlin, 1992).
[13] P. G. Jones, H. Rumpel, E. Schwarzmann, and G. M. Sheldrick, Acta Crystallogr., Sect. B: Struct. Crystallogr. Cryst. Chem. **35**, 1435 (1979).
[14] E. Schwarzmann, J. Mohn, and H. Rumpel, Z. Naturforsch. B **31B**, 135 (1976).
[15] E. Schwarzmann and G. Gramann, Z. Naturforsch. B **25B**, 1308 (1970).
[16] D. H. Parker and B. E. Koel, J. Vac. Sci. Technol. A **8**, 2585 (1990); M. A. Lazaga, D. T. Wickham, D. H. Parker, G. N. Kastanas, and B. E. Koel, ACS Symp. Ser. **523**, 90 (1993).
[17] N. Saliba, D. H. Parker, and B. E. Koel, Surf. Sci. **410**, 270 (1998).
[18] D. E. King, J. Vac. Sci. Technol. A **13**, 1247 (1995).
[19] A. Krozer and M. Rodah, J. Vac. Sci. Technol. A **15**, 1704 (1997).
[20] D. D. Eley and P. B. Moore, Surf. Sci. **76**, L599 (1978).
[21] T. Dickinson, A. F. Povey, and P. M. A. Sherwood, J. Chem. Soc., Faraday Trans. 1 **71**, 298 (1975).
[22] M. Peuckert, F. P. Coenen, and H. P. Bonzel, Surf. Sci. **141**, 515 (1984).
[23] Y. T. Kim, R. W. Collins, and K. Vedam, Surf. Sci. **233**, 341 (1990).
[24] K. Juodkazis, J. Juodkazyte, V. Jasulaitiene, A. Lukinskas, and B. Sebeka, Electrochem. Commun. **2**, 503 (2000).
[25] C. R. Aita and N. C. Tran, J. Vac. Sci. Technol. A **9**, 1498 (1991).
[26] L. Maya, M. Paranthaman, T. Thundat, and M. L. Bauer, J. Vac. Sci. Technol. B **14**, 15 (1996).
[27] A. M. Klumb, C. R. Aita, and N. C. Tran, J. Vac. Sci. Technol. A **7**, 1697 (1989).
[28] J. J. Pireaux, M. Liehr, P. A. Thiry, J. P. Delrue, and R. Caudano, Surf. Sci. **141**, 221 (1984).
[29] H. Ron and I. Rubenstein, Langmuir **10**, 4566 (1994).
[30] J. M. Gottfried, N. Elghobashi, S. L. M. Schroeder, and K. Christmann, Surf. Sci. **523**, 89 (2003).
[31] G. Kresse and J. Hafner, Phys. Rev. B **47**, 558 (1993); **49**, 14251 (1994).
[32] G. Kresse and J. Furthmüller, Comput. Mater. Sci. **6**, 15 (1996); Phys. Rev. B **54**, 11169 (1996).
[33] G. Kresse and D. Joubert, Phys. Rev. B **59**, 1758 (1999).
[34] J. P. Perdew, J. A. Chevary, S. H. Vosko, K. A. Jackson, M. R. Pederson, D. J. Singh, and C. Fiolhais, Phys. Rev. B **46**, 6671 (1992).
[35] E. Wimmer, H. Krakauer, M. Weinert, and A. J. Freeman, Phys. Rev. B **24**, 864 (1981).
[36] A. Canning, W. Mannstadt, and A. J. Freeman, Comput. Phys. Commun. **130**, 233 (2000).
[37] R. Asahi, W. Mannstadt, and A. J. Freeman, Phys. Rev. B **59**, 7486 (1999).
[38] R. Asahi, W. Mannstadt, and A. J. Freeman, Phys. Rev. B **62**, 2552 (2000).
[39] D. M. Bylander and L. Kleinman, Phys. Rev. B **41**, 7868 (1990).
[40] A. Seidl, A. Görling, P. Vogl, J. A. Majewski, and M. Levy, Phys. Rev. B **53**, 3764 (1996).
[41] L. Hedin, Phys. Rev. **139**, A796 (1965).
[42] W. X. Li, C. Stampfl, and M. Scheffler, Phys. Rev. B **65**, 075407 (2002).
[43] M. Fuchs, M. Bockstedte, E. Pehlke, and M. Scheffler, Phys. Rev. B **57**, 2134 (1998).
[44] B. D. Yu and M. Scheffler, Phys. Rev. B **56**, R15569 (1997).
[45] L. L. Wang and H. P. Cheng, Phys. Rev. B **69**, 165417 (2004).
[46] C. Kittel, *Introduction to Solid State Physics* (Wiley, New York, 1996).
[47] K. P. Huber and G. Herzberg, *Molecular Spectra and Molecular Structure IV: Constants of Diatomic Molecules* (Van Nostrand Reinhold, New York, 1979).
[48] J. P. Perdew, K. Burke, and M. Ernzerhof, Phys. Rev. Lett. **77**, 3865 (1996).
[49] A. Filippetti and V. Fiorentini, Phys. Rev. B **72**, 035128 (2005).
[50] *The Oxide Handbook*, edited by G. V. Samsonov (IFI/Plenum, New York, 1982).
[51] *Handbook of Chemistry and Physics*, edited by R. C. Weast, M. J. Astle, and W. H. Beyer, (CRC, Boca Raton, FL, 1988), Vol. 69.
[52] O. Kubaschewski, C. B. Alcock, and P. J. Spencer, *Materials Thermochemistry* (Pergamon, Oxford, 1993).
[53] D. R. Stull and H. Prophet, *JANAF Thermochemical Tables*, 2nd ed. (U.S. National Bureau of Standards, Washington, DC, 1971).
[54] M. Scheffler, in *Physics of Solid Surfaces*, edited by Vol. J.

Koukal (Elsevier, Amsterdam, 1988), p. 115.
[55] M. Hybertsen and S. G. Louie, Comments Condens. Matter Phys. **13**, 5 (1987).
[56] W. X. Li, C. Stampfl, and M. Scheffler, Phys. Rev. B **67**, 045408 (2003).
[57] L. H. Tjeng, M. B. J. Meinders, J. van Elp, J. Ghijsen, G. A. Sawatzky, and R. L. Johnson, Phys. Rev. B **41**, 3190 (1990).
[58] We considered value of U of 4.5, 5.3, 3.5, 4.0, 5.0, and 8.0 eV.